Vehicle Underhood Environment Investigations Using a Simplified Test Rig

Citation for the original published paper (version of record):
Vdovin, A., Sathiyan, T. (2023). Vehicle Underhood Environment Investigations Using a Simplified Test Rig. Energies, 16(24). http://dx.doi.org/10.3390/en16248028

energies

MDPI

Article

Vehicle Underhood Environment Investigations Using a Simplified Test Rig

Alexey Vdovin * and Tarun Kadri Sathiyan

Department of Mechanics and Maritime Sciences (M2), Division of Vehicle Engineering and Autonomous Systems (VEAS), Chalmers University of Technology, SE-412 96 Göteborg, Sweden; tarun.sathiyan@chalmers.se
* Correspondence: alexey.vdovin@chalmers.se

Abstract: Energy efficiency and thermal management continue to be critical areas in the vehicle development process. Independent of whether it is a vehicle with an internal combustion engine, hybrid, or fully electrical, engineers require proper and accurate tools to comprehend heat transfer in engine bays. However, developing such tools using a fully detailed production geometry can be challenging. This work presents a simplified and flexible test rig design of the vehicle underhood environment in two different variants: a passenger car and a commercial truck. The rig design in CAD and experimental data for the two rig configurations are made available upon request. These data will allow for the validation of different simulation approaches against the experimental dataset. An example of such a validation is presented in this paper. The load case scenario represented includes constant speed driving under heavy loads continued by a complete halt, which is followed by soaking for 100 min. The differences in experimental results for different rig variants are shown and analyzed. A good correlation between the experiments and CFD is obtained.

Keywords: CFD; thermal management; underhood flow; engine test rig; testing

Citation: Vdovin, A.; Kadri Sathiyan, T. Vehicle Underhood Environment Investigations Using a Simplified Test Rig. *Energies* **2023**, *16*, 8028. https://doi.org/10.3390/en16248028

Academic Editors: Daniela Anna Misul, Simone Salvadori and Mauro Carnevale

Received: 30 October 2023
Revised: 23 November 2023
Accepted: 8 December 2023
Published: 12 December 2023

1. Introduction

Vehicle manufacturers throughout the world are constantly struggling with reducing emissions and increasing the range of their vehicles. Simultaneously, the deadlines call for shorter development times considering technical progress from the concept phase to the final product to facilitate faster product deliveries to the market. To achieve this, extensive physical testing, which is expensive, must be reduced to a minimum. This can be accomplished by using various simulation techniques. Virtual methods offer the benefit of being relatively less expensive while having a faster turnaround time. However, to replace physical testing with virtual methods, these methods need to be both verified and validated.

Advanced research on underhood cooling of engine compartments is primarily based on numerical simulations to optimize cooling flow. There has been some research on optimizing engine bay flows using Computational Fluid Dynamics (CFD) simulations [1]. Most of such research works include real full-scale vehicles with highly detailed underhood compartments [2,3]. A major obstacle in numerically simulating the underhood cooling environment is the intricacy of engine components and their corresponding locations. A substantially detailed underhood environment is challenging to replicate, and it is also challenging to obtain consistent results both numerically and experimentally due to the complexities in the geometry as well as vehicle-specific designs.

To facilitate the design process, these sorts of detailed simulations can be further improved by adding virtual elements, e.g., [4]. In this research, detailed underhood components are covered by a virtual encapsulation box. Such a study is deemed to be challenging to validate or conduct experimental analysis. There are variations in approaches to simulating the detailing in the engine compartment, as shown in a similar research work [5]. However, the numerically obtained results again lack validation against experiments.

The most effective solution to obtaining results from numerical and experimental analysis is to develop a simplified engine test rig. The research work [6] showcases a highly simplified engine bay on which both experimental and numerical tests were conducted, studying both thermal and air flow aspects of the rig at soak conditions. In relation to [6], a 1D approach was also taken to understand the thermal soak process [7]. These studies were further developed to include top opening slots to allow air to leave the underhood enclosure [8,9]. Additionally, to investigate not only the soak but the driving scenario as well, the fan needs to be included. For example, in [10], a simplified rig with partial optical access to the engine bay was constructed. However, this rig enables aerodynamic flow analysis without considering any thermal characteristics of the engine compartment. Correspondingly, another work [11] involves a simplified and modular test rig containing sufficient detailing in the engine bay with complete optical access that investigated various grille shutter opening designs for cooling performance using CFD simulations as well as wind-tunnel tests. Like previous cases, this rig only included the aerodynamic aspect of the underhood environment and not thermal characteristics.

To investigate both aerodynamic and thermal aspects of the vehicles' underhood environments and facilitate the development of the CAE method of simulation techniques, rigs with sufficient detailing in the engine parts are required. Furthermore, the rig must contain generic components that are minimal and not specific to any vehicle. This allows the rig's geometry to be used in research with the possibility of reproducing the results. A good example of such a test rig was introduced in [12], where a soak test rig was developed to validate thermal soak CAE methods. Similarly, another rig was previously presented by the authors in [13]. In the work, a simplified vehicle underhood test rig with optical access was used to investigate engine bay air flows and temperature history of various parts. The constructed rig has a balance between sufficient detailing in the parts of the engine while maintaining a modular enclosure, which allows for various designs to be analyzed.

In contrast to previous work, which focused on introducing the rig and looking at a single configuration, this paper expands on the modularity perspective. The modularity of the rig permits different outlet designs and locations for different vehicles to be studied. This work focuses on the truck configuration of the test rig along with comparisons of two different rig variants (i.e., a passenger car and a commercial truck design). Variations in the geometry, along with their effects on the resulting flow field and temperature distributions, are presented from both experimental as well as numerical studies.

2. Experimental Setup

2.1. Test Rig Summary and Configurations

This study uses a previously constructed simplified vehicle engine bay for aerodynamic and thermal investigations [13]. To have easy optical access, the rig has modular glass walls. These walls can be used in several different configurations. For this study, two variants are analyzed (i.e., a car and a truck configuration), as shown in Figure 1. The air outlets or openings are represented in red. For the car configuration, three openings are present: two on the sides (measuring at 100 mm at the base and 150 mm in height) representing the openings to the wheelhouses and one at the back (measuring 220 × 175 mm) of the engine bay. For the truck configuration, only two openings exist. The large opening to the side (measuring 146 × 387 mm) replicates the opening towards the gearbox at the back of the cab, and the other opening at the rear, which is not changed, represents other ventilation paths. The total internal dimensions of the rig are 1090 × 660 × 542 mm. In both configurations, the inlet through which air enters the rig is the whole front end, where the fan and radiator are located. An additional difference between the variants is that the car configuration includes an aluminum heat shield on one side of the manifold.

Figure 1. An illustration of the test rig in two configurations: (**a**) a passenger car variant and (**b**) a commercial truck variant.

A simplified engine is represented by several "hot" and "cold" parts. Hot parts, see Figure 2, are made of copper and consist of a catalyst, a collector, a manifold, an exhaust pipe, and a turbo. Each of these components contains individual groups of heaters inside (shown in red) that are controlled manually to bring part surface temperatures to the desired levels. Cold parts, which are made of aluminum, mainly consist of an engine block, a circular and rectangular rod (and a heat shield for the car configuration case). These parts do not contain any heaters and are only passively heated by three means of heat transfer (i.e., conduction, convection, and radiation [14]) inside the test rig.

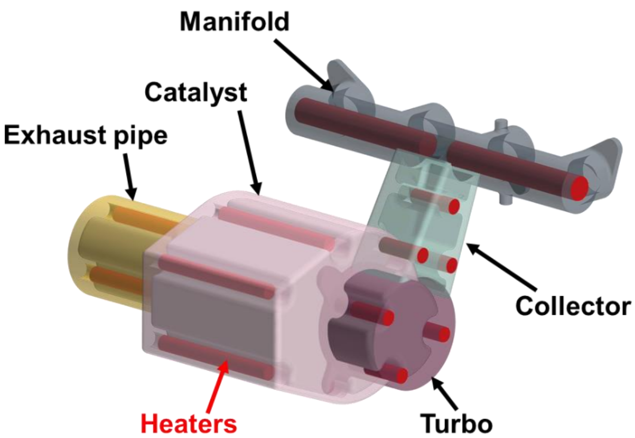

Figure 2. Five hot parts and heater positions inside them.

To measure the part temperatures, a total of 66 thermocouples (labeled TK1-TK66) are used; see Figure 3 for an example of the installation. TK1 to TK15 are located on the hot parts, whereas thermocouples on cold parts are marked from TK16 to TK32. All these thermocouples are embedded into the surfaces of the corresponding parts. The rest of the TKs are responsible for monitoring the internal heater temperatures and the temperatures of the glass walls. These TKs are not covered in this paper; however, the results are available and can be shared upon request.

Figure 3. An example of embedded thermocouples installation.

2.2. Experimental Procedure

The experimental procedure can be divided into two phases, namely, heat-up and cool-down phase. For the vehicle, these phases correspond to a test cycle of driving under heavy loads and then coming to a standstill. At the beginning of the test cycle, the fan is running at 2000 rpm, and the ceramic heaters are switched on. These heaters are manually controlled per hot part (i.e., 5 groups representing 5 hot parts) based on instantaneous temperature readings from the TKs embedded into heaters. The heater output per group is increased until the temperature of the first heater inside the corresponding part reaches the target. For this study, the heater target temperatures for the catalyst and exhaust pipe are 580 °C, and for the turbo, collector, and manifold, they are 740 °C. When one of the heaters per group reports the corresponding target temperature, the heat-up phase is completed.

To resume and initialize the main part of the test (i.e., the cool-down phase), all the heaters, along with the fan, are switched off. The convection heat transfer scenario rapidly changes from forced into natural. This leads to radiation heat transfer playing a larger role, and the rig goes into a state of thermal soak. Throughout this phase, the TK temperatures are constantly monitored and recorded for at least the first 100 min.

3. Numerical Setup

As stated earlier, the main use case scenario for the test rig is to enable the development and validation of different simulation approaches. These approaches can help design efficient engine bays and thermal protection for the internal components. The idea is to replicate the flow and temperature fields effectively using coupled aerodynamic and thermal simulations to facilitate an accurate heat-transfer prediction. An example of such an approach is given here, where the fundamental governing equations of fluid dynamics are solved in the computational domain using the Star-CCM+ 2302 software package.

3.1. Rig Model and Mesh

To perform the simulations, the CAD of the original test rig is further simplified by removing parts that are considered irrelevant to both flow and temperature fields inside the rig, e.g., the aluminum frame and support beams. The rig is placed in the computational domain that is sufficiently large for the boundary conditions to not produce an effect on the results obtained. The size used for the computational domain can be seen in Figure 4. All domain boundaries except the top are simulated as walls with a constant temperature of 28 °C which is represented in blue. The top (shown in red), representing ventilation in the room, is simulated using a pressure outlet boundary condition using the same temperature for the air backflow. Additionally, 28 °C is selected as it was the average ambient air temperature measured inside the room during the physical tests.

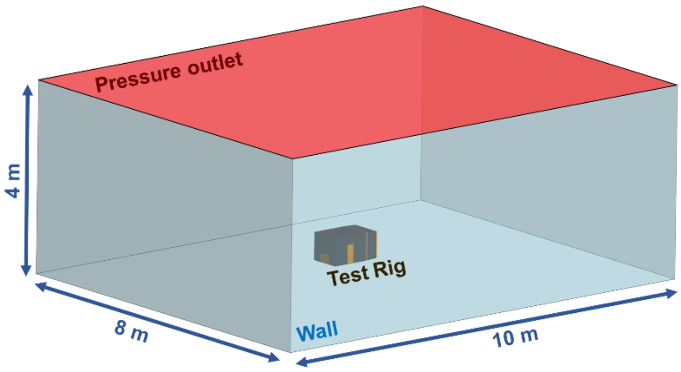

Figure 4. Size of the computational domain and boundary conditions used.

The air inside the domain and all essential solids (such as the heaters, hot parts, cold parts, and radiators) are meshed using best practice recommendations followed by a mesh study to ensure a mesh-independent solution. The resulting mesh is shown in Figure 5. The domain is split into regions to better control different settings and the mesh, which is indicated by different colors. Air regions are shown in blue and predominantly meshed using hexahedral cells; the only exception is the fan region where blade rotation is simulated using a multiple reference frame (MRF) approach [15]. Two radiators, shown in yellow, are modeled as porous regions. Lastly, to enable simulation of the heat conduction through parts, all of them are also meshed using a solid mesh, which is represented by the pink color. The final mesh contains around 14 million cells for fluids and 7 million cells for solids.

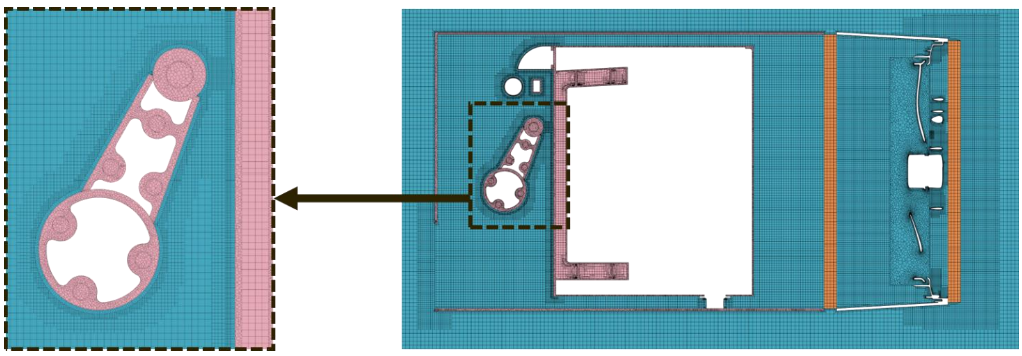

Figure 5. A section cut through the mesh at the center of the rig.

3.2. Simulation Approach

During the heat-up phase in experiments, the heaters are manually controlled, which results in significant variations in heat-up curves between the repetitions of the same test. Consequently, the heat-up phase is not simulated, and the initial conditions for the cool-down simulations are calculated using a steady-state Reynolds–Averaged Navier–Stokes (RANS) approach. The air is modeled as an ideal gas with the realizable k-epsilon model used for turbulence [16].

The timeline for the cool-down simulations is shown in Figure 6. The first minute, where a lot of changes in the flow field occur, is simulated using unsteady RANS (URANS) when both flow and energy are resolved. For the rest of the simulation, a semi-transient approach is applied, i.e., the flow solver is periodically frozen to allow solving temperature fields using larger time steps compared to the time steps required for the flow solver. Periodically, the flow field is updated to account for the new part temperatures. A more detailed description of the simulation setup and individual settings for the components and materials used can be found in the following publication [13].

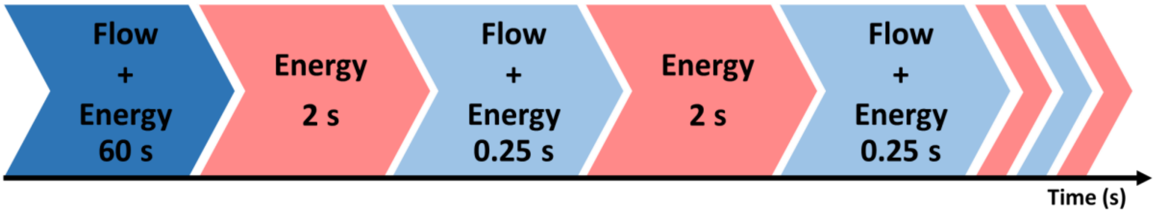

Figure 6. Simulation timeline.

4. Results and Discussions

This chapter comprises a detailed analysis of the experimental results of the test rig by comparing the two different configurations, i.e., commercial truck and passenger car. Furthermore, simulation results are validated against experiments. Only results from the first 32 thermocouples that are located on the metal parts (i.e., both hot and cold parts) are analyzed and compared between the two configurations of the test rig, as these are the most crucial. The exact positions of these TKs are depicted in Figure 7.

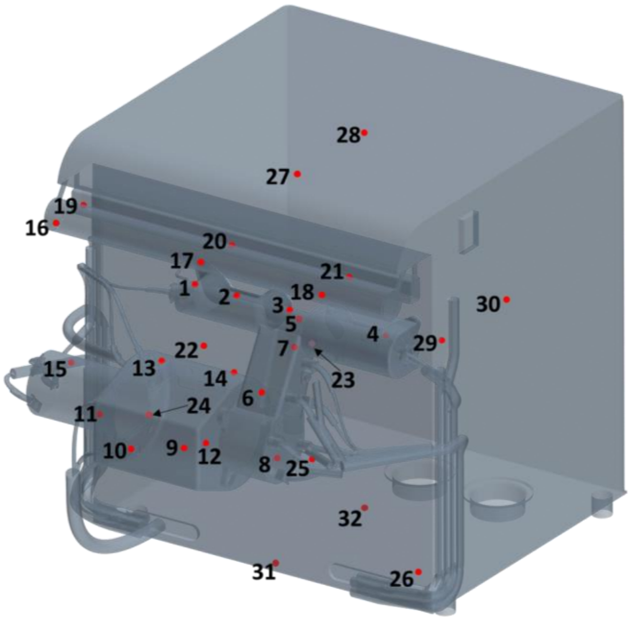

Figure 7. Thermocouple positions on the metal parts of the rig.

4.1. Comparison of Different Rig Variant Results

4.1.1. Experimental Average Temperature at Start of Soak

For experimental analysis and to ensure repeatable results, the same test is performed several times for each configuration of the test rig. However, an average of all the experimental results for the respective test rig configuration is considered to simplify the comparison study. Figure 8 shows the experimental average thermocouple temperatures right before the start of the soak.

The above figure shows that overall temperatures after the heat-up phase on both the hot and cold parts of the test rig in the truck configuration are relatively higher than those of the car configuration. It should also be noted that while the same maximum heater temperature per part is used as a target, the heater's output is slightly different between the two rig variants, resulting in differences of up to ±6%.

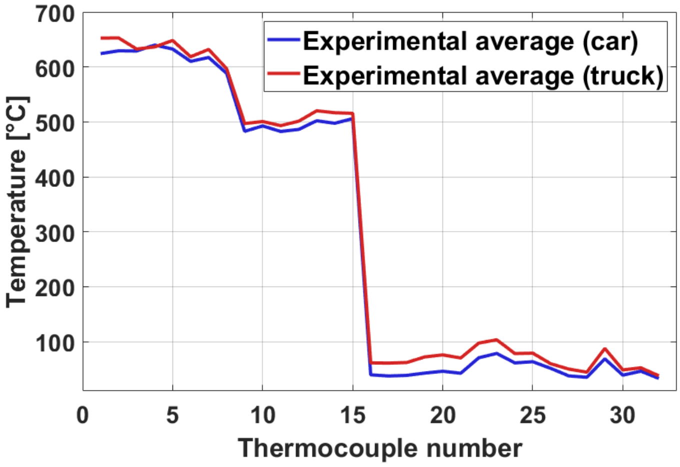

Figure 8. Thermocouple temperatures before the start of soak for two configurations.

The hot parts (i.e., TK1-TK15) have slightly higher temperatures for the truck configuration due to flow stagnations within the glass walls, as there are no outlets on one side of the test rig for the truck configuration, which leads to air recirculation or stagnant air in that part of the rig. On the other hand, the cold parts (i.e., circular and rectangular rods, TK16-TK21) are also seen to be significantly warmer for the truck configuration relative to the car. This is due to the presence of a heat shield in the car configuration and the absence of it in the truck configuration. The heat shield affects the radiation heat transfer from the manifold to the cold parts. The comparison for surface temperatures of the engine block (i.e., TK22-TK32) also shows a slight increase in temperature for truck configuration.

4.1.2. Experimental Cool-Down Curves

Figure 9 shows the comparison of the cool-down curves between car and truck configurations of the test rig for thermocouple (TK3) located on the manifold surface in the middle of the manifold, away from the heat shield. The curves match relatively well, with minor deviations from each other. This is due to the flow variations between the car and truck configurations caused by differences in the number of outlets, outlet size, and outlet positions.

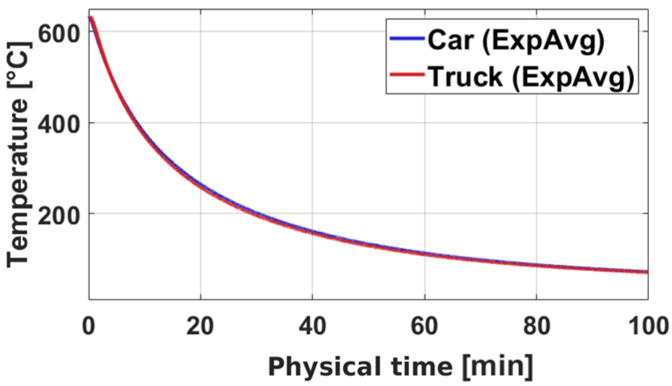

Figure 9. Cool-down curves of TK3 (middle of the manifold, away from the heat shield) for car and truck configurations.

Furthermore, a comparison of the cool-down curves of the thermocouple (TK21), which are located on the surface of a cold part (i.e., circular rod) right above the heat shield, is shown in Figure 10. It is clearly seen that the temperature of the cold part rises for approximately 10 minutes into the soaking phase, which is an expected behavior, as seen in similar studies [12]. As this thermocouple is located above the heat shield, it is evident that the truck configuration gets warmer than the car configuration. The reason behind this increase in temperature is radiation heat transfer from the hot part (i.e., manifold) to the cold part (i.e., circular rod) in case of the truck configuration where the heat shield is not present. This is further confirmed by a significant difference in temperatures at the beginning of the soak.

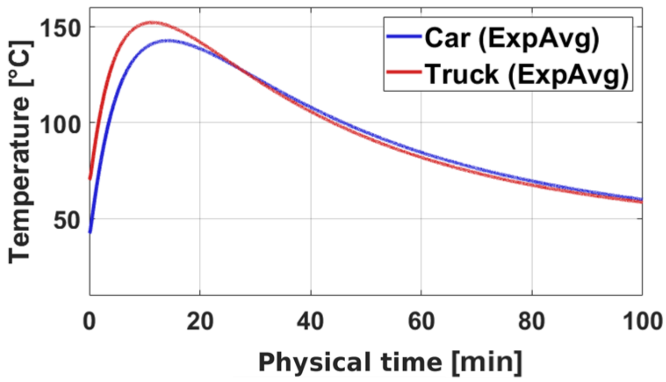

Figure 10. Cool-down curves of TK21 (the cold part right above the heatshield) for car and truck configurations.

4.2. Comparison Study between Simulations and Experimental Results for the Truck Configuration

4.2.1. Part Temperatures at the Start of Soak

To check the credibility of numerical results, surface temperatures from simulations before the start of soak are compared to experimental average temperatures reported from all thermocouples; see a plot in Figure 11. The temperatures of hot parts (i.e., TK1-TK15) correlate well; however, deviations are seen in temperatures reported from cold parts (TK16-TK32).

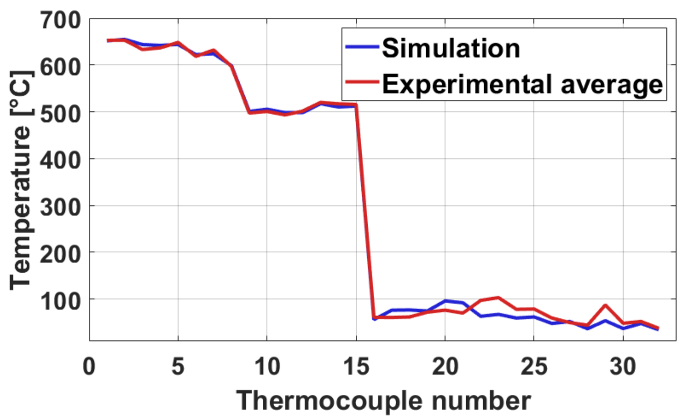

Figure 11. Average experimental thermocouple temperatures against simulation before the start of the soak.

4.2.2. Transient Soak Simulations

The natural convection plume formation for the first 20 s of soaking is shown in Figure 12 using a vertical cut plane at the middle of the rig. Time 0 s represents the air temperatures after the heaters are turned off and the fan completely stops. Consequently, there is no more cool air being forced into the test rig, i.e., there is no forced convection. This leads to the heating up of the air around the hot parts and the beginning of plume formation due to buoyancy effects, effects which are seen clearly at 10 s and even more at the 20 s mark. This plume carries energy away from hot parts while heating up the rest of the rig.

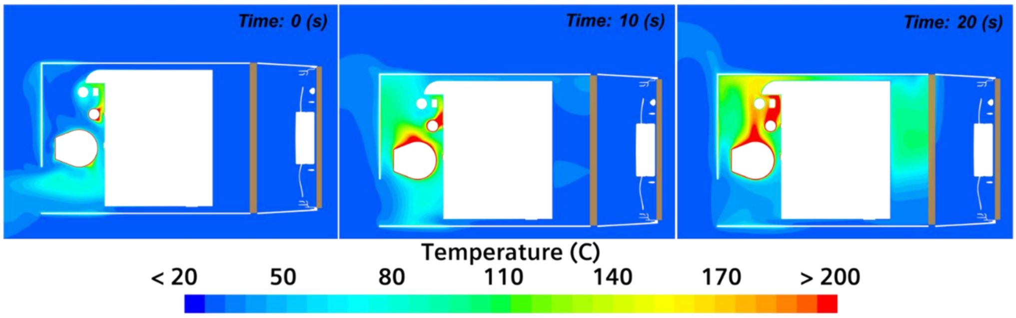

Figure 12. Stages of natural convection plume formation for the truck configuration shown on the vertical center plane.

Figure 13 shows a volumetric rendering of the air temperatures inside and around the test rig for the truck configuration after 130 s of soaking. It is apparent that warm air accumulates at the top of the test rig. The warm air can be seen venting out through the large side opening and eventually through the front of the rig after passing the two radiators. To cool off the hot parts quicker, ideally, there must be some openings at the top of the setup, e.g., [8,9]. This would allow faster recirculation of air in the domain and faster cooldown.

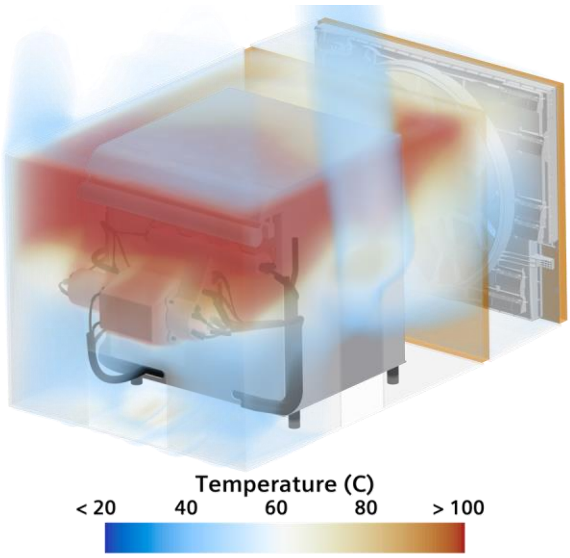

Figure 13. Volumetric rendering of air temperature after 130 s of soak.

Considering the simulation results for the temperature history of different parts, two examples of the cool-down curves are presented in Figure 14. The graphs represent TK1 (located on the hot manifold) and TK20 (located on the cold rectangular rod). Temperatures of the hot parts (TK1 in this case) drop rapidly after the fan and heaters are turned off. The behavior of the cool-down curves for the cold parts (e.g., TK20) is a bit more complex. As the forced convection cooling ceases, radiation from hot parts and increasing air temperatures result in cold parts becoming hotter, at least during the first 10 min. Later, as the energy is being dissipated into the environment, the temperatures start to drop.

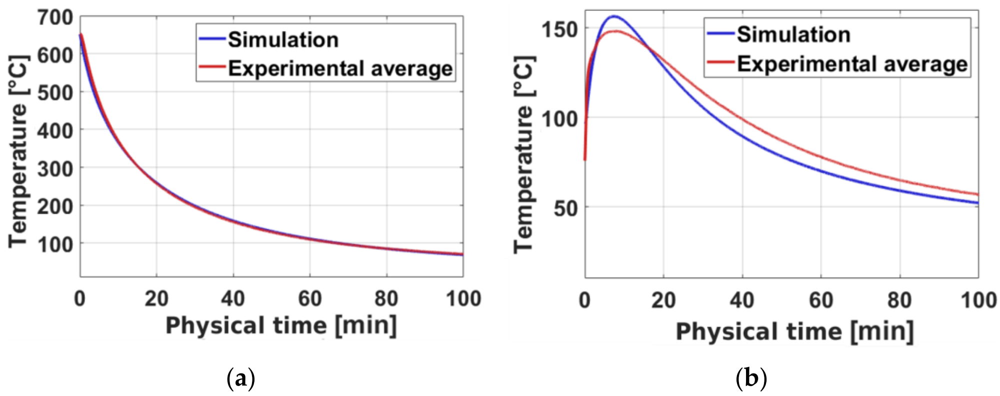

Figure 14. Example cool-down curves of hot (**a**) and cold (**b**) parts.

The simulation results correlate well with experimentally obtained values, especially for the hot parts. In the case of cold parts, some discrepancies can be observed. However, it should be noted that the temperature scale of the graph is significantly different, the peak in temperature is achieved at approximately the same time, and the slopes of the curves are very similar. Another notable observation is that the simulation overestimates the peak temperature compared to the experimental average, which still indicates the areas that require further investigation from the underhood design perspective. In this case, the maximum TK20 temperature is overestimated by about 8 °C. In a corresponding car case, TK20 also showed one of the highest overestimations of peak temperatures among TKs located on cold parts, ending up with an overprediction of 14 °C [13].

5. Conclusions

This study exhibits two variants of the simplified vehicle underhood test rig. The differences in geometries, along with their effects on the flow field and part surface temperatures, are investigated. As the temperatures of the hot parts are controlled during the heat-up phase, starting temperatures before soaking are relatively consistent. However, the flow field inside the rig is significantly affected by the different openings between variants. Nevertheless, it is observed that the cool-down curves for hot parts of the rig show almost identical behavior during the soaking phase, independent of the rig variant. On the flip side, the cool-down curves for the cold parts experience minor divergences. These are mostly caused by the presence of a heat shield in the car configuration case and its absence in the truck variant case. This difference results in higher radiation heat transfer from the hot manifold surface to the cold parts located in the vicinity. This leads to a higher initial temperature prior to soaking and higher peak temperatures during the soak.

In addition to evaluating the two rig variants, an example of the primary usage scenario for all the data generated utilizing the test rig is described. Coupled aerodynamic and thermal simulations are performed using a semi-transient CFD approach. The results of the simulations are used to investigate the changes in the flow field and variations in part temperatures during the soak. The results show that the temperature evolution for the hot parts is predicted accurately. However, temperature prediction of cold parts during soak shows marginal overprediction of peak temperatures from simulations. Nonetheless, the overall curve behavior estimate is acceptable. It is shown that the numerical method can help predict the overheating of sensitive components in the underhood environment, thus leading to efficient design strategies.

This paper only presents a subset of the total experimental database generated by the tests conducted with the rig. This is due to both the car and truck variants being tested under different starting temperature conditions for the soak. A more complete experimental dataset, including the CAD of the test rig, can be made available upon request.

Author Contributions: Conceptualization, A.V. and T.K.S.; methodology, A.V. and T.K.S.; software, A.V. and T.K.S.; validation, A.V. and T.K.S.; formal analysis, A.V. and T.K.S.; investigation, A.V. and

T.K.S.; resources, A.V.; data curation, A.V. and T.K.S.; writing—original draft preparation, A.V. and T.K.S.; writing—review and editing, A.V. and T.K.S.; visualization, A.V. and T.K.S.; supervision, A.V.; project administration, A.V.; funding acquisition, A.V. All authors have read and agreed to the published version of the manuscript.

Funding: The computations are enabled by resources provided by the National Academic Infrastructure for Supercomputing in Sweden (NAISS) and the Swedish National Infrastructure for Computing (SNIC) at National Supercomputer Centre (NSC) and Chalmers' Centre for Computational Science and Engineering (C3SE) partially funded by the Swedish Research Council through grant agreements no. 2022-06725 and no. 2018-05973. This research and APC was funded by Strategic Vehicle Research and Innovation (FFI) grant number P44920-1.

Data Availability Statement: Data will be made available upon request.

Acknowledgments: The authors would like to acknowledge Volvo Car Corporation as well as Volvo Truck Technology for their significant contribution into designing and building the rig. Ammar Hazim Saber is acknowledged for his contribution to obtaining the experimental results.

Conflicts of Interest: The authors declare that they have no known competing financial interests or personal relationships that could have appeared to influence the work reported in this paper.

References

1. Schuetz, T.C. *Aerodynamics of Road Vehicles*, 5th ed.; SAE International: Warrendale, PA, USA, 2015. [CrossRef]
2. Shim, H.R.; Park, J.M. *A Study of The Transient Analysis Technique on the under Hood Thermal Damage*; SAE Technical Papers; SAE International: Warrendale, PA, USA, 2011. [CrossRef]
3. Zhang, C.; Uddin, M.; Robinson, A.C.; Foster, L. Full vehicle CFD investigations on the influence of front-end configuration on radiator performance and cooling drag. *Appl. Therm. Eng.* **2018**, *130*, 1328–1340. [CrossRef]
4. Minovski, B.; Andrić, J.; Löfdahl, L.; Gullberg, P. A numerical investigation of thermal engine encapsulation concept for a passenger vehicle and its effect on fuel consumption. *Proc. Inst. Mech. Eng. Part D J. Automob. Eng.* **2019**, *233*, 557–571. [CrossRef]
5. Kula, S.; Bulut, E.; Altay, E.; Sümer, O.; Oztürk, F. Smart cooling design using dual loop cooling to increase engine efficiency and decrease fuel emissions with artificial intelligence. *Case Stud. Therm. Eng.* **2022**, *40*, 102351. [CrossRef]
6. Wang, Z.; Han, J.; Mukutmoni, D. *Numerical Simulation of Unsteady Natural Convection in a Simplified Engine Bay Enclosure under Soak Conditions*; SAE Technical Papers; SAE International: Warrendale, PA, USA, 2014. [CrossRef]
7. Minovski, B.; Löfdahl, L.; Andrić, J.; Gullberg, P. A Coupled 1D–3D Numerical Method for Buoyancy-Driven Heat Transfer in a Generic Engine Bay. *Energies* **2019**, *12*, 4156. [CrossRef]
8. Chen, K.H.; Johnson, J.; Merati, P.; Davis, C. Numerical investigation of buoyancy-driven flow in a simplified underhood with open enclosure. *SAE Int. J. Passeng. Cars–Mech. Syst.* **2013**, *6*, 805–816. [CrossRef]
9. Minovski, B.B.; Lofdahl, L.; Gullberg, P. *Numerical Investigation of Natural Convection in a Simplified Engine Bay*; SAE Technical Papers; SAE International: Warrendale, PA, USA, 2016. [CrossRef]
10. Khaled, M.; Gad El Rab, M.; Hachem, F.; Elhage, H.; Elmarakbi, A.; Harambat, F.; Peerhossaini, H. Experimental study of the flow induced by a vehicle fan and the effect of engine blockage in a simplified model. *Int. J. Automot. Technol.* **2016**, *17*, 617–627. [CrossRef]
11. Franzke, R.; Sebben, S.; Willeson, E. Experimental investigation of the air flow in a simplified underhood environment. *Proc. Inst. Mech. Eng. Part D J. Automob. Eng.* **2021**, *236*, 2272–2282. [CrossRef]
12. Sweetman, B.; Schmitz, I.; Hupertz, B.; Shaw, N.; Goldstein, J. Experimental and Numerical Investigation of Vehicle Drive and Thermal Soak Conditions in a Simplified Engine Bay. *SAE Int. J. Passeng. Cars–Mech. Syst.* **2017**, *10*, 433–445. [CrossRef]
13. Vdovin, A.; Sathiyan, T.K.; Duwig, C.; Saber, A.H. A Test Rig for the Validation of CFD Simulations of a Passenger Vehicle Under Hood Environment. *SSRN* **2023**. [CrossRef]
14. Bergman, T.L.; Lavine, A.S.; Incropera, F.P.; DeWitt, D.P. *Fundamentals of Heat and Mass Transfer*; John Wiley & Sons: Hoboken, NJ, USA, 2018.
15. Siemens Digital Industries Software. *Simcenter STAR-CCM+ User Guide, version 2302*; Siemens Digital Industries Software: Plano, TX, USA, 2023.
16. Menter, F.R. Two-equation eddy-viscosity turbulence models for engineering applications. *AIAA J.* **1994**, *32*, 1598–1605. [CrossRef]